Covalently bound substrate at the regulatory site triggers allosteric enzyme activation

Steffen Kutter[1], Manfred S. Weiss[2], Georg Wille[1§], Ralph Golbik[1], Michael Spinka[1],

Stephan König[1†]

Abstract

The mechanism by which the enzyme pyruvate decarboxylase from yeast is activated allosterically has been elucidated. A total of seven three-dimensional structures of the enzyme, of enzyme variants or of enzyme complexes from two yeast species (three of them reported here for the first time) provide detailed atomic resolution snapshots along the activation coordinate. The prime event is the covalent binding of the substrate pyruvate to the side chain of cysteine 221, thus forming a thiohemiketal. This reaction causes the shift of a neighbouring amino acid, which eventually leads to the rigidification of two otherwise flexible loops, where one of the loops provides two histidine residues necessary to complete the enzymatically competent active site architecture. The structural data are complemented and supported by kinetic investigations and binding studies and provide a consistent picture of the structural changes, which occur upon enzyme activation.

Introduction

The two closely related pyruvate decarboxylases from *Saccharomyces cerevisiae* (*Sc*PDC) and *Kluyveromyces lactis* (*Kl*PDC) are well-characterised thiamine diphosphate (ThDP) dependent enzymes, which share 86.3 % identical amino acid residues. They have been studied in great detail by means of kinetic investigations of the native enzymes[1-4] of

[†1]Institute for Biochemistry & Biotechnology, Faculty for Biological Sciences, Martin-Luther-University Halle-Wittenberg, Kurt-Mothes-Str. 3, 06120 Halle (Saale), Germany. [2]European Molecular Biology Laboratory Outstation, c/o DESY, Notkestr. 85, 22603 Hamburg, Germany. [§]Present address: Institute for Biophysics, Dept. Physics, Johann-Wolfgang-Goethe-University Frankfurt/Main, Max-von-Laue-Str. 1, 60438 Frankfurt/Main

catalytically active variants and of catalytically almost inactive variants of *Sc*PDC, like D28A or E477Q[5-12]. They display an allosteric substrate activation behaviour, which they share with PDCs from plant seeds[13-17]. Consequently, sigmoidally shaped *v*/S plots result. At substrate concentrations around $S_{0.5}$ (the equivalent value to K_m for enzymes with hyperbolic *v*/S plots) a considerable time period (~60 s at 30 ºC) elapses before catalysis is accelerated and the steady state is entered[18]. The observed activation rate constants rise with increasing substrate concentration. In contrast, the PDC from the bacterium *Zymomonas mobilis* (*Zm*PDC)[19] and indolepyruvate decarboxylase from *Enterobacter cloacae* (*Ec*IPDC)[20] show Michaelis-Menten type kinetics without any sign of substrate activation.

A number of substrate surrogates have been identified, which are able to activate PDC as well. The effects of pyruvamide (PA) on the activation kinetics have been studied in detail for *Sc*PDC[1] and *Kl*PDC[4]. Phosphonate analogues (among them methyl acetylphosphonate, MAP) of pyruvate have been applied to elucidate the catalytic cycle[21-25] or to trap reaction intermediates in crystal structures[26-28].

PDCs are multi-subunit enzymes dependent on the cofactor thiamine diphosphate (ThDP), which is bound mainly via a divalent metal ion, magnesium in most cases, to the protein component. The typical molecular mass of the subunit is 59-61 kDa. The catalytically active state of most PDCs is the tetramer, but higher oligomers (octamers, hexadecamers) have also been described for PDCs from plant seeds[14,15] or some fungi[29]. Crystal structures are known for *Sc*PDC[30] for *Kl*PDC[31], for *Sc*PDC activated by PA[32] and ketomalonate[33], respectively, and for two non-activated species, *Zm*PDC[34] and *Ec*IPDC[35]. All three-dimensional structures display a very high similarity on the basis of monomers and dimers (for an early comparison see Muller *et al.*[36]). Monomers consist of three domains, each with an open α/β topology, 5-6 stranded β-sheets are surrounded by α-helices. Domains are connected by long, in some cases flexible loop regions. The cofactor ThDP is bound between two monomers. Each N-terminal (PYR-) domain binds the aminopyrimidine part of the cofactor, each C-terminal (PP-) domain

the corresponding diphosphate part via the divalent metal ion, generating the vital V-conformation of the cofactor ThDP[37]. The proposed ThDP binding motif is found in all PDCs analysed so far[38]. Because of this cofactor-binding mode monomers are associated very tightly within one dimer with a large interface area[34]. Significant differences between PDC crystal structures manifest themselves at the tetramer stage. *Sc*PDC without bound ligands forms an open tetramer[30], whereas *Sc*PDC crystallised in the presence of the substrate surrogate PA forms a half-side closed tetramer[32]. A half-side closed conformation was also found for *Kl*PDC in the absence of any ligand[31]. Hence, the mode of tetramer arrangement does not appear to be the critical feature of the activation mechanism. Instead, it is the flexibility of two loop regions near the catalytic site of PDC, which seems to be different between activated and non-activated enzyme species. These loop regions, comprising residues 104-113 and 288-304 (identical numbering for *Kl*PDC and *Sc*PDC, for sequence details see supplemental figure 1), have never been detected in crystal structures of native PDCs due to their inherent disorder[30,31]. For the side chains of the adjacent residues H114 and H115 very poor electron density was found, indicating high flexibility. However, in the crystal structure of PA activated *Sc*PDC, the loops become at least ordered at one side of the tetramer[32]. The binding of ligands at the regulatory site of the enzyme affects the efficiency of catalysis by initiating conformational changes of the protein structure. Although the catalytic cycle of PDCs has been analysed in great detail by kinetic studies of enzyme variants[6,10,11,39-44] along with intermediate analyses[45,46,47] and studies of the effect of cofactor analogues[48-54], information on the mechanistic basis of allosteric regulation is rather scarce. Chemical modification of PDCs with group specific reagents pointed to an important role of cysteine residues[55]. The number of cysteines and their reactivity was determined by derivation with 4-hydroxy mercuribenzoate and 3-bromopyruvamide, respectively[56]. Site directed mutagenesis of cysteine residues to alanine or serine demonstrated that residue C221 might be the decisive one for enzyme activation[7,8,57-59]. Consequently, it was postulated that the region around C221

is the regulatory site of PDC. The question remained, however, how the signal is transferred to the active site. Kinetic studies on a number of variants favour a direct pathway through neighbouring amino acid side chains to the cofactor ThDP[9,60].

First insights into the structural background of substrate activation of PDCs came from small angle X-ray solution scattering (SAXS) studies and X-ray crystal structure analysis. The artificial substrate surrogate PA was used with both methods. The presence of PA in enzyme solutions led to a significant increase of the radius of gyration (R_G). This suggested a global conformational change of the enzyme molecule in solution[61]. In the crystal structure of PA-ScPDC the binding of the activator at the regulatory site caused a rotation of two dimers relative to each other within the tetramer. However, PA was found in half of the regulatory and active sites only and not directly bound to C221, but 10 Å away instead. Consequently, only half of the flexible loop regions became ordered[32].

Here, we present the crystal structures of KlPDC with the bound substrate surrogate methyl acetylphosphonate (MAP, for chemical structures, see supplemental figure 2) and of the ScPDC variants D28E and E477Q with bound substrate pyruvate (PYR) together with detailed kinetic studies on the activating effect of both activators and binding studies using the SAXS method. With this knowledge in hand it is now possible to comprehensively describe the mechanism of allosteric activation of PDCs.

Results and Discussion

Kinetic effects of MAP

As MAP was used as a substrate surrogate in crystallographic studies on KlPDC it was important to demonstrate that this analogue does indeed act as an activator of this enzyme. In the absence of any effectors KlPDC displays typical sigmoidal steady state kinetics[4]. After incubation of the enzyme with MAP the sigmoidicity of the *v/S*-plot becomes gradually suppressed with increasing concentrations of this surrogate (Fig. 1A). At an MAP

concentration of 75 mM the enzyme's steady state kinetics is essentially hyperbolic. Moreover, at pyruvate concentrations below 1 mM the activating effect of MAP is also documented by the higher absolute values of the steady state rates (inset of Fig. 1A). This effect is even more apparent from the corresponding progress curves (Fig. 1B). In the absence of MAP the progress curves of KlPDC show lag phases, which reflect the conversion of the initial inactive enzyme state into the activated enzyme state[4]. Upon pre-incubation of KlPDC with MAP the initial reaction rate (v_0) is increased. Eventually, at a MAP concentration of 75 mM the progress curve appears to be a straight line in accordance with the hyperbolic v/S plots obtained under these conditions (Fig. 1A). Initial rates (v_0) and steady state rates (v_{SS}) can be evaluated from empirical progress curves (for details, see Krieger $et\ al.$[4]). The plot of the ratio v_0/v_{SS} $versus$ MAP concentration (Fig. 1C) clearly demonstrates that MAP is able to completely activate KlPDC. This is in contrast to what is observed for the substrate surrogate PA, which accounts for upper values of 0.65 for v_0/v_{SS} in comparable kinetic experiments[4]. For MAP a half saturation value of 37 mM can be extracted from the sigmoidal fit in Fig. 1C. Time-dependent pre-incubation studies revealed that the MAP-triggered activation of KlPDC is a rather slow process as compared to the activation by its native substrate pyruvate (Fig. 1D). In presence of MAP substrate saturation is reached at somewhat higher substrate concentrations (Fig. 1A), pointing to a weak competitive inhibition by this effector. Accordingly, MAP binds non-covalently to the active site of KlPDC as shown below. In summary, the kinetic data presented here demonstrate that MAP is an activator for yeast PDCs, thus justifying its application in crystallographic studies. A kinetic study, which will present a detailed model, is in progress.

Direct activator binding studies using SAXS

It had been demonstrated earlier[61] that addition of PA to ScPDC resulted in a significant increase of the radius of gyration (R_G), the scattering parameter describing the maximum distance of two points within a particle in solution. These changes in R_G had been interpreted

as global rearrangement (dimer rotation) within the protein molecule without altering the oligomerisation state of the enzyme (because of the unchanged scattering intensity I(0), which correlates with the molecular mass of the particle). Here we illustrate, to the best of our knowledge for the first time, the activator concentration dependence of R_G for the binding of PA and MAP to KlPDC and of the substrate pyruvate to the variant ScPDC$_{E477Q}$. All plots exhibit a clear saturation of the ligand binding (Fig. 2). Binding constants can be drawn directly from sigmoid fits of the experimental data. As shown in Fig. 2, MAP and PA have similar binding affinities for KlPDC (20 and 30 mM, respectively) and for ScPDC (data not shown). However, by far the highest affinity is found for the native substrate pyruvate with a value of 6 mM along with the highest increase of R_G. The lowest shift of R_G was found after binding of PA. Notably, the values for the binding affinities of MAP drawn from activation kinetics and SAXS binding studies, respectively, conform closely to each other. This indicates that both methods monitor the same process.

Structural implications

Overall structures

The crystal structure of KlPDC in complex with MAP was determined to 2.3 Å resolution, those of the ScPDC variants in complex with pyruvate to 1.7 Å (D28A) and 1.4 Å resolution (E477Q), respectively (for data collection, processing and refinement statistics see table 1). The final models comprise four times 562 amino acid residues, each of the subunits harbouring one cofactor molecule ThDP, one Mg^{2+} and 2 molecules of activator (in case of MAP three additional molecules per tetramer could be pasted). The asymmetric units contain the PDC tetramer. The overall folds of the subunits within one dimer (Fig. 3A) are almost identical to that of native species (KlPDC, r.m.s.d. 2.28 Å for 1116 superimposed Cα-atoms, ScPDC$_{E477Q}$, r.m.s.d. 0.97 Å for 1074 superimposed Cα-atoms, ScPDC$_{D28A}$, r.m.s.d. 0.96 Å for 1074 superimposed Cα-atoms). Differences were found at the surface of the tetramer, i.e. at the middle domains and the C-terminal α-helices. The MAP molecules are located at the

active sites of *Kl*PDC with distances of 2.22 Å between the Cα-atoms of MAP and the C2

atoms of ThDP within one tetramer, and at the regulatory sites, covalently bound to C221

(bond length 1.82 Å). Pyruvate molecules are found with distances of 1.69 Å (Cα-C2) at the

active sites and 2.12 Å at the regulatory sites in *Sc*PDC$_{D28A}$, and with distances of 2.04 Å to

C221 of *Sc*PDC$_{E477Q}$, but not in the active sites of the latter variant. The absence of pyruvate

in the active site of *Sc*PDC$_{E477Q}$ might be associated with the disrupted cofactor molecule

(exposed thiazolium ring) in this species. The tetramers of MAP-*Kl*PDC, PYR-*Sc*PDC$_{D28A}$

and PYR-*Sc*PDC$_{E477Q}$ are superimposable without significant differences (r.m.s.d. of 0.5-0.6

Å for 2248 Cα-atoms).

Comparison of the new crystal structures with that of PA activated ScPDC

A comparison of these structures with the structure of PA activated *Sc*PDC shows that the

latter exhibits a tilted dimer-dimer arrangement in the tetramer and that the activator is non-

covalently bound at the regulatory site, 10 Å away from C221. Furthermore, only half of all

activator sites are occupied. The differences between the activation capabilities of PA on one

hand, and MAP and pyruvate on the other are corroborated by many other studies on the

mechanism of activation. In contrast to MAP and pyruvate, PA is not able to activate PDCs

completely. Progress curves of PDC catalysis always show lag phases, even in the presence of

high concentrations of PA[4].

Loop structuring

The most salient feature common to all activated structures described herein is the well-

defined electron density for two loop regions (residues 104-113 and 288-304, respectively,

Fig. 3A), which is virtually absent in the crystal structure of native *Sc*PDC[30] or poorly defined

in the structure of native *Kl*PDC[31] (Fig. 3B). It may therefore be postulated that loop

structuring and loop translocation are the decisive events in the activation process. The gained

rigidity of both loop regions at all subunits within the tetramer enforces the planar and

symmetric dimer arrangement within the tetramer. Both loops are located in the

neighbourhood to the active site (Fig. 3). In the frozen state these loop regions are stabilized internally by a number of H-bonds (Supplemental table 1). Loop 104-113 additionally develops a short α-helix and closes partially over the active site. H114 and H115, the next upstream neighbours of loop 104-113, are part of the active site. Especially for H114 an essential function in PDC catalysis has been proposed from kinetic studies with accordant variants form yeast and bacteria[10,11,39,44]. Tittmann *et al.*[46] postulated a specific role for H114 (together with D28) during release of the reaction product acetaldehyde.

Regulatory site

The most striking result of this study is the evidence for a covalent C-S bond at the side chain of C221 in the activated structures, which finally confirms results of studies on the activation mechanism by chemical modification[55,56] and mutation of cystein residues[7,8,57-59] in *Sc*PDC. The covalent character of this bond is well documented by the crystallographic C-S distance (1.82 Å) as well as by the tetrahedral configuration at the former carbonyl carbon of both MAP (Fig. 4A) and pyruvate (Fig. 4B). Notably, the sp^3 character of the Cα-atom of pyruvate in both activated *Sc*PDC variants is somewhat less developed than that of the equivalent carbon atom in the MAP-activated *Kl*PDC. Together with the longer distances between the Cα-atom of pyruvate and the Cβ-atom of C221, this could be indicative of a dynamic equilibrium of non-covalently and covalently bound pyruvate at the regulatory site. Apart from C221, the following residues are located in vicinity (within 5 Å distance) to the bound activator (for MAP-*Kl*PDC): H92, R161, H225, G286, A287, L288, H310, S311, Y313, M326 and 5 waters. Thus, the regulatory site is predominantly lined by positively charged side chains, which can interact electrostatically with the phosphonate moiety of MAP or the carboxylate moiety of pyruvate, respectively, as well as with their corresponding thiohemiketals. Surprisingly, H-bonds are only formed from main chain carbonyl oxygen atoms of G286 and A287 to the α-hydroxyl group (the former carbonyl group) of the covalently bound MAP.

Effects on the active site

Interestingly, almost all side chains constituting the active site apart from D28, H114 and H115 remain unaffected by the binding of the activators at C221. Furthermore, no significant distortion of the cofactor's vital V-conformation is seen in the activated state. However, a comparison of the native and the MAP-activated crystal structures of *Kl*PDC revealed that the two amino acids H114 and H115 undergo marked structural reorientations upon activator binding (Fig. 5). The histidine side chains are now directed towards the substrate-binding site, i. e. the distances of their ring nitrogens to the C2 atom of the cofactor ThDP are diminished from 12-15 Å to 6-7 Å. Concomitantly, the main chain of residue D28/A28 is rotated by ~35° and the side chain is orientated towards H115. This reorientation basically restructures the active site into its enzymatically competent architecture - triggered by activator binding at C221.

Signal transfer from the thiohemiketal at C221 to the active site

The question of how the signal of activation is transmitted from C221 to the active site is a matter of debate that has not been decided to this very date. What can be drawn about signal transduction from the new structures? Firstly, the formation of the thiohemiketal at C221, which itself is not part of either loop (Fig. 6B), shifts the side chain of this amino acid about 4 Å from its original position in the native structures. Secondly, this shift induces the translocation of A287 by 4 Å (Fig. 6C), thereby rigidifying the loop 288-304 (Fig 6D). Thirdly, the fixated loop 288-304 forms a number of interactions (Supplemental table 1) with the other, originally flexible loop 104-113, thereby becoming structured itself (Fig. 6E). The position of the latter is now identical to those in the three-dimensional structures of *Zm*PDC and *Ec*IPDC, which are not allosterically regulated species. Eventually, the signal is transmitted to H114 and H115, which adopt their new orientation in activated PDC (Fig. 5, 6F). Notably, residues E91 and W412 proposed to be pivotal side chains for the signal transduction in *Sc*PDC[9,60] does not experience any displacement in the activated structures.

However, it should be noted that the activation process does not necessarily require a distinct set of amino acids to push each other like billiard balls. Rather, activation represents a search process on the protein's free energy landscape[62], which becomes slightly distorted upon binding of effectors at C221, developing new interactions along the way until the activated state is reached. Thus, the molecule undergoes this conversion as an entirety, implying that also side chains that are not subject to any significant structural rearrangement might be dynamically important in the process. Therefore, the amino acids shown to be relevant by extensive kinetic and spectroscopic studies[7-9,60] keep playing their part.

Molecular causes of cofactor activation

Phenomenologically, the activation of *Sc*PDC and *Kl*PDC is reflected in lag phases of their respective progress curves as well as in the sigmoidal shape of the steady state kinetics[1,4]. Both enzyme species are potentially inactive at the start of the reaction[4,18]. A decade ago, Kern *et al.*[45] have shown that the first step of activation in *Sc*PDC is the deprotonation at the C2 atom of thiamine diphosphate, which requires a tremendous shift of the pKa value of the C2 proton to become catalytically competent[63]. The structural basis of this kinetic effect remained, however, largely elusive. Evidently, some structural differences between the active sites in the native and the activated state must account for the observed acceleration of the H/D exchange at the cofactor's C2 atom as triggered by activation in both yeast PDCs. The results of the current crystallographic study allow some preliminary insight. First and foremost, the active site is complete only in the activated state. A vital role has been ascribed to H113 in *Zm*PDC, as part of a catalytic dyad supporting aldehyde release[40,46]. Its position is equivalent to that of H114 in *Sc*PDC and *Kl*PDC, respectively, which reorients upon activation. Both histidines, H114 and H115, are required for efficient catalysis. Moreover, the H114F/H115F variant, though being almost inactive, shows perfect Michaelis-Menten behaviour, pointing to abolished activation[10]. These observations, however, do not yet explain the accelerated deprotonation at the C2 atom of the cofactor, as neither H114 nor H115 are

specifically involved in this process. Secondly, the structured loops, particularly the region 104-113, shield the active site against the solvent. Thus, the microenvironment of the cofactor is probably less polar in the activated than in the native state. As a non-polar environment dramatically promotes deprotonation at the C2 atom of the cofactor[64], the partial closure of the active site might well be the decisive molecular cause of the cofactor's activation. Thirdly, solvent shielding might likewise contribute to the stabilization of non-polar reaction intermediates as e.g. the enamine and, additionally, promote the general sequestration of substrates and intermediates. On the other hand, substrate molecules must have access to the active site during catalysis. Therefore, the active site cannot be totally shielded from the solvent. It should be noted that even the rigidified loop structures retain a considerable measure of mobility, which allows substrate access. It remains to be clarified, whether a quasi-periodic closure and re-opening of the active site in the activated state is coupled to particular stages of the catalytic cycle as advocated by Kluger & Smyth[65] or is even synchronised with a dynamic alternation between covalently and non-covalently associated pyruvate at C221 as proposed by Alvarez et al.[3] and defended recently by Schowen[66]. Finally, the question might be raised, why nature chose thiohemiketal formation, a rare mode of covalent modification, which is, to the best of our knowledge, unique as principle of enzyme regulation. It might be speculated that thiohemiketal formation was favoured as pyruvate lacks an extended hydrophobic moiety that could function as a partner in non-covalent ligand-protein interaction.

Methods Summary

The enzymes were purified to homogeneity by using established protocols, *Kl*PDC according to Kutter et al.[31], the others according to Killenberg-Jabs et al.[6].

The enzyme complexes were crystallised using the vapour diffusion technique with hanging drops[31]. For cryoprotection of crystals 1:1 mixtures of reservoir and PEG400 or glycerol were

applied. Diffraction data were collected at synchrotron beamlines. Standard programs were used for data treatment. Structures were solved by molecular replacement. Model building and evaluation was done with the program WINCOOT[67,68].

Protein concentration was determined spectrophotometrically.

Catalytic activities were measured via a coupled optical test with NADH/ScADH[69] on a Jasco V-560 UV/VIS spectrophotometer.

SAXS data were collected at a synchrotron beamline[70]. The forward scattering intensity I(0) and radius of gyration (R_G) were calculated with the program GNOM[71].

Methods

Protein crystallisation

KlPDC was dissolved in 20 mM citrate buffer pH 6.1, 1 mM DTT, 5 mM ThDP, 5 mM MgSO$_4$, 80 mM MAP. The same solution without MAP, but with 7-23 % (w/v) PEG 2000/PEG 6000 (1:1 ratio) as precipitant was used as reservoir. Well diffracting crystals were obtained after 10 days equilibration at 8 °C at 20 % PEG and 1 mg KlPDC per mL. Stored stock solutions of ScPDC variants were diluted into 12 mM citrate/1,33 mM MES pH 6.35, 1.33 mM DTT, 1.33 mM ThDP, 1.33 mM MgSO$_4$, 630 mM pyruvate, 5 µg/mL ScADH, 2 mM NADH+H$^+$. A buffer containing 18 mM citrate/2 mM MES pH 6.35, 2 mM DTT, 2 mM ThDP, 2 mM MgSO$_4$ together with 7-24 % (w/v) PEG 2000/PEG 6000 (1:1 ratio) was used as reservoir solution. Well diffracting crystals resulted from these batches after 14 days of incubation at on ice at PEG concentration of 22.5 % (w/v) and 1 mg enzyme per mL.

Data collection, structure determination and refinement

For cryoprotection crystals were incubated in a 1:1 mixture of reservoir and an aqueous solution of 32-42 %(w/v) PEG400 and 5 %(v/v) glycerol for 1 min (in case of MAP-KlPDC, 10-15 s). Diffraction data were collected at the beamlines X12 (EMBL Outstation Hamburg, c/o Desy), and ID14-2 (ESRF, Grenoble). For indexing, integration and scaling the programs

DENZO und SCALEPACK[72] were used. Intensities were converted to structure factor amplitudes using the program TRUNCATE[73]. *Kl*PDC (PDB ID code, 2G1I) was used as search model for the MAP-*Kl*PDC-complex, and PA-*Sc*PDC (PDB ID code, 1QPB) for the PYR-*Sc*PDC$_{D28A}$-complex and the latter for the PYR-*Sc*PDC$_{E477Q}$-complex. Refinement was realised with the program REFMAC5[73].

Protein concentration

Whenever possible, the protein concentration was determined spectrophotometrically from the UV-spectra at 280 nm (Jasco V-560 UV/VIS spectrophotometer) using a molar extinction coefficient of 60,000 $M^{-1} \cdot cm^{-1}$ for one PDC subunit. In all other cases the Bradford method[74] was applied.

Kinetic measurements

0.05 M MES buffer pH 6.0, 0.15 M ammonium sulphate and an observation wavelength of 355 nm were applied. The corresponding extinction coefficient for NADH at this wavelength was determined to be 4764 $M^{-1} \cdot cm^{-1}$.

Small-angle X-ray solution scattering (SAXS) with synchrotron radiation

Measurements were performed at beamline X33 at the EMBL Hamburg outstation, DESY, Hamburg (camera length 2.7 m, MAR345 image plate detector, vacuum sample cell) at 16 °C and at protein concentrations of ~2.5 mg/mL. The buffer system was the same as used for kinetic measurements, but 2 mM DTT were added. The momentum transfer axis s ($s=4\pi\sin\theta/\lambda$, where 2θ is the scattering angle and $\lambda=0.15$ nm, the X-ray wavelength) was calibrated using collagen or tripalmitin as standards. The scattering patterns were collected for 120 s. MAR image files were extracted during data collection for intensity normalization (transmitted flux, detector response, scaling of the s-axis) by the data reduction program AUTOMAR[75]. Buffer scattering was subtracted using the program PRIMUS-MAR[76]. The molecular masses were obtained from the ratio of the forward scattering intensity of the samples and that of the molecular mass standard bovine serum albumin.

Acknowledgement

We would like to thank the Jordan group at Rutgers for the variants D28A and E477Q, Brigitta Seliger for preparation of the enzyme species from *S. cerevisiae,* and Anja Seidel and Robert Eckensthaler for crystallisation of MAP-*Kl*PDC. Access to EMBL X12 beamline at the DORIS storage ring, DESY, Hamburg and to beamline ID14-2 at the ESRF in Grenoble is acknowledged.

References

1. Hübner, G., Weidhase, R. & Schellenberger, A. The mechanism of substrate activation of pyruvate decarboxylase: A first approach. *Eur. J. Biochem.* **92**, 175-181 (1978).

2. König, S., Hübner, G. & Schellenberger, A. Cross-linking of pyruvate decarboxylase. Characterization of the native and substrate-activated states. *Biomed. Biochim. Acta* **49**, 465-471 (1990).

3. Alvarez, F.J., Ermer, J., Hübner, G., Schellenberger, A. & Schowen, R.L. The linkage of catalysis and regulation in enzyme action, solvent isotope effects as probes of protonic sites in the yeast pyruvate decarboxylase mechanism. *J. Am. Chem. Soc.* **117**, 1678-1683 (1995).

4. Krieger, F., Spinka, M., Golbik, R., Hübner, G. & König, S. Pyruvate decarboxylase from *Kluyveromyces lactis* - An enzyme with an extraordinary substrate activation behaviour. *Eur. J. Biochem.* **269**, 3256-3263 (2002).

5. Killenberg-Jabs, M., König, S., Hohmann, S. & Hübner, G. Purification and characterisation of the pyruvate decarboxylase from a haploid strain of *Saccharomyces cerevisiae*. *Biol. Chem. Hoppe-S.* **377**, 313-317 (1996).

6. Killenberg-Jabs, M., König, S., Eberhardt, I., Hohmann, S. & Hübner, G. Role of Glu51 for cofactor binding and catalytic activity in pyruvate decarboxylase from yeast studied by site-directed mutagenesis. *Biochemistry* **36**, 1900-1905 (1997).

7. Baburina, I. *et al.* Substrate activation of brewer's yeast pyruvate decarboxylase is abolished by mutation of cysteine 221 to serine. *Biochemistry* **33**, 5630-5635 (1994).

8. Baburina, I., Li. H., Bennion, B., Furey, W. & Jordan, F. Interdomain information transfer during substrate activation of yeast pyruvate decarboxylase: The interaction between cysteine 221 and histidine 92. *Biochemistry* **37**, 1235-1244 (1998).

9. Li, H., Furey, W. & Jordan, F. Role of glutamate 91 in information transfer during substrate activation of yeast pyruvate decarboxylase. *Biochemistry* **38**, 9992-10003 (1999).

10. Liu, M. *et al.* Catalytic acid-base groups in yeast pyruvate decarboxylase. 1. Site-directed mutagenesis and steady-state kinetic studies on the enzyme with the D28A, H114F, H115F, and E477Q substitutions. *Biochemistry* **40**, 7355-7368 (2001).

11. Sergienko, E.A. & Jordan, F. Catalytic acid-base groups in yeast pyruvate decarboxylase. 2. Insights into the specific roles of D28 and E477 from the rates and stereospecificity of formation of carboligase side products. *Biochemistry* **40**, 7369-7381 (2001).

12. Joseph, E., Wie, W., Tittmann, K. & Jordan, F. Function of a conserved loop of the beta-domain, not involved in thiamin diphosphate binding, in catalysis and substrate activation in yeast pyruvate decarboxylase. *Biochemistry* **45**, 13517-13527 (2006).

13. Davies DD (1967) Glyoxylate as a substrate for pyruvic decarboxylase. Proc Biochem Soc 104, 50P

14. Zehender, H., Trescher, D. & Ullrich, J. Improved purification of pyruvate decarboxylase from wheat germ. Its partial characterization and comparison with the yeast enzyme. *Eur. J. Biochem.* **167**, 149-154 (1987).

15. Mücke, U., König, S. & Hübner, G. Purification and characterisation of pyruvate decarboxylase from pea seeds (*Pisum sativum* cv. Miko). *Biol. Chem. Hoppe-S.* **376**, 111-117 (1995).

16. Dietrich, A. & König, S. Substrate activation behaviour of pyruvate decarboxylase from *Pisum sativum* cv. Miko. *FEBS Lett.* **400**, 42-44 (1997).

17. Acar, S., Yücel, M. & Hamamci, H. Purification and characterisation of two isozymes of pyruvate decarboxylase from *Rhizopus oryzae*. *Enzyme Microb. Technol.* **40**, 675-682 (2007).

18. Hübner, G. & Schellenberger, A. Pyruvate decarboxylase - potentially inactive in the absence of the substrate. *Biochem. Internat.* **13**, 767-772 (1986).

19. Bringer-Meyer, S., Schimz, K.L. & Sahm, H. Pyruvate decarboxylase from *Zymomonas mobilis*. Isolation and partial characterization. *Arch. Microbiol.* **146**, 105-110 (1986).

20. Schütz, A. *et al.* Studies on structure-function relationships of indolepyruvate decarboxylase from *Enterobacter cloacae* - a key enzyme of the indole acetic acid pathway. *Eur. J. Biochem.* **270**, 2322-2331 (2003).

21. Biryukov, A.I., Bunik, V.I., Zhukov, Y.N., Khurs, E.N. & Khomutov, R.M. Succinyl phosphonate inhibits alpha-ketoglutarate oxidative decarboxylation, catalyzed by alpha-ketoglutarate dehydrogenase complexes from *E. coli* and pigeon breast muscle. *FEBS Lett.* **382**, 167-170 (1996).

22. Bunik, V.I., Biryukov, A.I. & Zhukov, Y.N. Inhibition of pigeon breast muscle alpha-ketoglutarate dehydrogenase by phosphonate analogues of alpha-ketoglutarate. *FEBS Lett.* **303**, 197-201 (1992).

23. Kluger, R. & Nakaoka, K. Inhibition of acetoacetate decarboxylase by ketophosphonates. Structural and dynamic probes of the active site. *Biochemistry* **13**, 910-914 (1974).

24. Kluger, R. & Pike, D.C. Active site generated analogs of reactive intermediates in enzymic reactions. Potent inhibition of pyruvate dehydrogenase by a phosphonate analog of pyruvate. *J. Am. Chem. Soc.* **99**, 4504-4506 (1977).

25. O'Brien, T.A., Kluger, R., Pike, D.C. & Gennis, R.B. Phosphonate analogues of pyruvate. Probes of substrate binding to pyruvate oxidase and other thiamin pyrophosphate-dependent decarboxylases. *Biochim. Biophys. Acta* **613**, 10-17 (1980).

26. Arjunan, P. *et al.* A thiamin-bound, pre-decarboxylation reaction intermediate analogue in the pyruvate dehydrogenase E1 subunit induces large scale disorder-to-order transformations in the enzyme and reveals novel structural features in the covalently bound adduct. *J. Biol. Chem.* **281**, 15296-15303 (2006).

27. Bera, A.K. *et al.* Mechanism-based inactivation of benzoylformate decarboxylase, a thiamin diphosphate-dependent enzyme. *J. Am. Chem. Soc.* **129**, 4120-4121 (2007).

28. Wille, G. *et al.* The catalytic cycle of a thiamin diphosphate enzyme examined by cryocrystallography. *Nat. Chem. Biol.* **2**, 324-328 (2006).

29. Alvarez, M.E. *et al.* The 59-kDa polypeptide constituent of 8-10-nm cytoplasmic filaments in *Neurospora crassa* is a pyruvate decarboxylase. *Gene* **130**, 253-258 (1993).

30. Arjunan, P. *et al.* Crystal structure of the thiamin diphosphate-dependent enzyme pyruvate decarboxylase from the yeast *Saccharomyces cerevisiae* at 2.3 Å resolution. *J. Mol. Biol.* **256**, 590-600 (1996).

31. Kutter, S. *et al.* The crystal structure of pyruvate decarboxylase from *Kluyveromyces lactis*. Implications for the substrate mechanism of this enzyme. *Febs J.* **273**, 4199-4209 (2006).

32. Lu, G., Dobritzsch, D., Baumann, S., Schneider, G. & König, S. The structural basis of substrate activation in yeast pyruvate decarboxylase - A crystallographic and kinetic study. *Eur. J. Biochem.* **267**, 861-868 (2000).

33. Furey, W. *et al.* Structure-function relationships and flexible tetramer assembly in pyruvate decarboxylase revealed by analysis of crystal structures. *Biochim. Biophys. Acta* **1385**, 253-270 (1998).

34. Dobritzsch, D., König, S., Schneider, G. & Lu, G. High resolution crystal structure of pyruvate decarboxylase from *Zymomonas mobilis*. Implications for substrate activation in pyruvate decarboxylases. *J. Biol. Chem.* **273**, 20196-20204 (1998).

35. Schütz, A. *et al.* Crystal structure of indolepyruvate decarboxylase from *Enterobacter cloacae*, an enzyme involved in the biosynthesis of the plant hormone indole-3-acetic acid. *Eur. J. Biochem.* **270**, 2312-2321 (2003).

36. Muller, Y.A. *et al.* A thiamin diphosphate binding fold revealed by comparison of the crystal structures of transketolase, pyruvate oxidase and pyruvate decarboxylase. *Structure* **1**, 95-103 (1993).

37. Pletcher, J., Sax, M., Turano, A. & Chang, C.H. Effects of structural variations in thiamin, its derivatives and analogues. *Ann. N.Y. Acad. Sci.* **378**, 454-458 (1982).

38. Hawkins, C.F., Borges, A. & Perham, R.N. A common structural motif in thiamin pyrophosphate-binding enzymes. *FEBS Lett.* **255**, 77-82 (1989).

39. Candy, J.M., Koga, J., Nixon, P.F. & Duggleby, R.G. The role of residues glutamate-50 and phenylalanine-496 in *Zymomonas mobilis* pyruvate decarboxylase. *Biochem. J.* **315**, 745-751 (1996).

40. Schenk, G., Leeper, F.J., England, P. & Duggleby, R.G. The role of His113 and His114 in pyruvate decarboxylase from *Zymomonas mobilis*. *Eur. J. Biochem.* **248**, 63-71 (1997).

41. Pohl, M., Siegert, P., Mesch, K., Bruhn, H. & Grötzinger, J. Active site mutants of pyruvate decarboxylase from *Zymomonas mobilis* - A site-directed mutagenesis study of L112, I472, I476, E473 and N482. *Eur. J. Biochem.* **257**, 538-546 (1998).

42. Chang, A.K., Nixon, P.F. & Duggleby, R.G. Aspartate-27 and glutamate-473 are involved in catalysis by *Zymomonas mobilis* pyruvate decarboxylase. *Biochem. J.* **339**, 255-260 (1999).

43. Sergienko, E.A. & Jordan, F. Catalytic acid-base groups in yeast pyruvate decarboxylase. 3. A steady-state kinetic model consistent with the behavior of both wild-type and variant enzymes at all relevant pH values. *Biochemistry* **40**, 7382-7403 (2001).

44. Huang, C.Y., Chang, A.K., Nixon, P.F. & Duggleby, R.G. Site-directed mutagenesis of the ionizable groups in the active site of *Zymomonas mobilis* pyruvate decarboxylase - Effect on activity and pH dependence. *Eur. J. Biochem.* **268**, 3558-3565 (2001).

45. Kern, D. *et al.* How thiamine diphosphate is activated in enzymes. *Science* **275**, 67-70 (1997).

46. Tittmann, K. *et al.* NMR analysis of covalent intermediates in thiamin diphosphate enzymes. *Biochemistry* **42**, 7885-7891 (2003).

47. Schütz, A., Golbik, R., König, S., Hübner, G. & Tittmann, K. Intermediates and transition states in thiamin diphosphate-dependent decarboxylases. A kinetic and NMR study on wild-type indolepyruvate decarboxylase and variants using indolepyruvate, benzoylformate, and pyruvate as substrates. *Biochemistry* **44**, 6164-6179 (2005).

48. Wittorf, H.J. & Gubler, C.J. Coenzyme binding in yeast pyruvate decarboxylase. Kinetic studies with thiamine diphosphate analogues. *Eur. J. Biochem.* **22**, 544-550 (1971).

49. Tomita, I., Saitou, S. & Ozawa, T. Coenzyme analogue inhibition in the reconstitution of yeast pyruvate decarboxylase and transketolase. *Biochem. Biophys. Res. Commun.* **57**, 78-84 (1974).

50. Golbik, R. *et al.* Function of the aminopyrimidine part in thiamine pyrophosphate enzymes. *Bioorg. Chem.* **19**, 10-17 (1991).

51. Eppendorfer, S. *et al.* Effects of metal ions, thiamin diphosphate analogues and subunit interactions on the reconstitution behaviour of pyruvate decarboxylase from brewer's yeast. *Biol. Chem. Hoppe-S.* **374**, 1129-1134 (1993).

52. Schellenberger, A., Hübner, G. & Neef, H. Cofactor designing in functional analysis of thiamin diphosphate enzymes. *Methods Enzymol.* **279**, 131-146 (1997).

53. Mann, S., Melero, C.P., Hawksley, D. & Leeper, F.J. Inhibition of thiamin diphosphate dependent enzymes by 3-deazathiamin diphosphate. *Org. Biomol. Chem.* **2**, 1732-1741 (2004).

54. Erixon, K.M., Dabalos, C.L. & Leeper, F.J. Inhibition of pyruvate decarboxylase from *Z-mobilis* by novel analogues of thiamine pyrophosphate: Investigating pyrophosphate mimics. *Chem. Commun.*, 960-962 (2007).

55. Brauner, T. & Ullrich, J. Yeast pyruvate decarboxylase. Number and reactivity of mercapto groups. *Hoppe-S. Z. Physiol. Chem.* **353**, 825-831 (1972).

56. Hübner, G., König, S. & Schellenberger, A. The functional role of thiol groups of pyruvate decarboxylase from brewer's yeast. *Biomed. Biochim. Acta* **47**, 9-18 (1988).

57. Zeng, X.P. *et al.* Role of cysteines in the activation and inactivation of brewers' yeast pyruvate decarboxylase investigated with a pdc1-pdc6 fusion protein. *Biochemistry* **32**, 2704-2709 (1993).

58. Wei, W., Liu, M. & Jordan, F. Solvent kinetic isotope effects monitor changes in hydrogen bonding at the active center of yeast pyruvate decarboxylase concomitant with substrate activation: The substituent at position 221 can control the state of activation. *Biochemistry* **41**, 451-461 (2002).

59. Wang, J. *et al.* Consequences of a modified putative substrate-activation site on catalysis by yeast pyruvate decarboxylase. *Biochemistry* **40**, 1755-1763 (2001).

60. Li, H. & Jordan, F. Effects of substitution of tryptophan 412 in the substrate activation pathway of yeast pyruvate decarboxylase. *Biochemistry* **38**, 10004-10012 (1999).

61. Hübner, G., König, S., Schellenberger, A. & Koch, M.H.J. An X-ray solution scattering study of the cofactor and activator induced structural changes in yeast pyruvate decarboxylase (PDC). *FEBS Lett.* **266**, 17-20 (1990).

62. McCammon, J.A. & Karplus, M. Simulation of protein dynamics. *Ann. Rev. Phys. Chem.* **31**, 29-45 (1980).

63. Washabaugh, M.W. & Jencks, W.P. Thiazolium C(2)-proton exchange: structure-reactivity correlations and the pKa of thiamin C(2)-H revisited. *Biochemistry* **27**, 5044-5053 (1988).

64. Crosby, J. & Lienhard, G.E. Mechanism of thiamine-catalyzed reactions. A kinetic analysis of the decarboxylation of pyruvate by 3,4-dimethylthiazolium ion in water and ethanol. *J. Am. Chem. Soc.* **92**, 5707-5716 (1970).

65. Kluger, R. & Smyth, T. Interaction of pyruvate thiamine diphosphate adducts with pyruvate decarboxylase. Catalysis through 'closed' transition states. *J. Am. Chem. Soc.* **103**, 1214-1216 (1981).

66. Schowen, R.L. Isotopic and other studies on the molecular origins of substrate regulation of some pyruvate decarboxylases: a reconsideration. *Isot. Environ. Health Stud.* **43**, 1-16 (2007).

67. Emsley, P. & Cowtan, K. Coot: model-building tools for molecular graphics. *Acta Crystallogr. D* **60**, 2126-2132 (2004).

68. Lohkamp, B., Emsley, P. & Cowtan, K. Coot News. *CCP4 Newsletter 42, Contribution 7* (2005).

69. Holzer, H., Schultz, G., Villar-Palasi, C. & Jüngten-Sell, J. Isolierung der Hefecarboxylase und Untersuchungen über die Aktivität des Enzyms in lebenden Zellen. *Biochem. Z.* **327**, 331-344 (1956).

70. Rössle, M.W. *et al.* Upgrade of the small-angle X-ray scattering beamline X33 at the European Molecular Biology Laboratory, Hamburg. *J. Appl. Crystallogr.* **40**, S190-S194 (2007).

71. Svergun, D.I. Determination of the regularization parameter in indirect transform methods using perceptual criteria. *J. Appl. Crystallogr.* **25**, 495-503 (1992).

72. Otwinowski, Z. & Minor, W. Processing of X-ray diffraction data collected in oscillation mode. *Methods Enzymol.* **276**, 307-326 (1997).

73. Collaborative Computational Project Number 4 CCP4 suite: programs for protein crystallography. *Acta Crystallogr. D* **50**, 760-763 (1994).

74. Bradford, M. A rapid and sensitive method for the quantitation of mircogram quantites of protein utilizing the principles of protein-dye binding. *Anal. Biochem.* **72**, 248-254 (1976).

75. Petoukhov, M.V., Konarev, P.V., Kikhney, A.G. & Svergun, D.I. ATSAS 2.1 - towards automated and web-supported small-angle scattering data analysis. *J. Appl. Crystallogr.* **40**, 223-228 (2007).

76. Konarev, P.V., Volkov, V.V., Sokolova, A.V., Koch, M.H.J. & Svergun, D.I. PRIMUS: a Windows PC-based system for small-angle scattering data analysis. *J. Appl. Crystallogr.* **36**, 1277-1282 (2003).

Table 1

Data collection and refinement statistics for MAP-*Kl*PDC, PYR-*Sc*PDC$_{D28A}$, PYR-*Sc*PDC$_{E477Q}$

Parameter	MAP-*Kl*PDC	PYR-*Sc*PDC$_{D28A}$	PYR-*Sc*PDC$_{E477Q}$
pdb ID	2VJY	2VK1	2VK8
Beamline	X12	ID14-2	ID14-2
Detector	MARCCD	ADSC Q4R CCD	ADSC Q4R CCD
Wavelength (Å)	0.93001	0.933	0.933
Temperature (K)	100	100	100
Crystal detector distance (mm)	220	125	101
Rotation range per image (°)	0.5	0.5	0.5
Total number of images	437	360	360
Resolution range (Å)	104.26-2.30	99.0-1.71	95.4-1.42
(Highest resolution shell)	(2.34-2.30)	(1.74-1.71)	(1.44-1.42)
Space group	P2$_1$	P2$_1$	P2$_1$
Unit cell parameters (Å, °)	a=81.76, b=135.77, c=107.26, β=103.88	a=80.88, b=141.31, c=114.41, β=107.19	a=78.98, b=190.51, c=84.14, β=113.01
Mosaicity (°)	0.79	0.38	0.40
Total number of reflections	438,157	937,903	1,523,231
Unique reflections	100,426	262,151	427,276
Redundancy	4.4	3.6	4.4
I/σ(I)	9.6 (2.3)	17.5 (2.1)	22.5 (1.9)
Completeness (%)	99.7 (99.9)	99.3 (99.2)	99.7 (99.8)
R$_{merge}$ (%)	14.8 (61.5)	6.8 (57.4)	5.3 (62.9)
R$_{r.i.m.}$ (%)	16.8 (70.6)	8.0 (68.0)	n.d.
R$_{p.i.m.}$ (%)	8.0 (34.3)	4.2 (36.1)	n.d.
Overall B-factor (Wilson plot, Å^2)	29.7	20.8	17.6

Parameter	MAP-*Kl*PDC	PYR-*Sc*PDC$_{D28A}$	PYR-*Sc*PDC$_{E477Q}$
Total number of used reflections	99345	260330	425935
Total number of atoms (non-hydrogen)	18588	18994	19242
Number of protein atoms	17344	17280	17292
Number of water molecules	1048	1558	1818
R$_{cryst}$ (%)	15.4 (19.2)	19.1 (24.8)	18.1 (25.4)
R$_{free}$ (%)	22.5 (30.5)	22.0 (27.6)	18.6 (26.7)
Total number of reflections for R$_{free}$	1006	1313	1068
Bond length (r.m.s.d. from ideality, Å)	0.025	0.018	0.013
Bond angles (r.m.s.d. from ideality, °)	1.95	1.45	1.25
Ramachandran plot (% in most favoured regions)	89.5	90.9	91.3
Ramachandran plot (% in allowed regions)	99.8	100	100
Average B-factor (Å^2)	26.3	20.9	18.9

Figure legends

Figure 1

MAP kinetics.

A, Influence of MAP on the shape of the *v/S* plot (black circles, 0 mM MAP, red squares, 20 mM MAP, green triangles, 40 mM MAP, and blue inverse triangles, 75 mM MAP). The lines represent sigmoid fits for 0 and 20 mM MAP and hyperbolic fits for 40 mM and 75 mM MAP, respectively. Inset, enlarged view at low substrate concentrations.

B, Transients of the *Kl*PDC catalysed reaction at 3 mM pyruvate (conditions as in **A**). For better comparison, original data are normalised to steady state rate and to the same initial absorbance.

C, dependence of the ratio of initial rate (v_0) and steady state rate (v_{SS}) on MAP concentration. The rates were obtained from transients (see B for examples)[4]. The line represents a sigmoid fit.

D, Activator concentration dependence of the apparent activation rate constant k_{obs} (circles, pyruvate, squares, MAP). The k_{obs} values were obtained from transients[4], in the presence of MAP a line is drawn for better visualisation only.

Figure 2

Dependence of the scattering parameter radius of gyration (R_G) of PDC on the concentration of the added activator.

In the case of PA and MAP, *Kl*PDC, in the case of pyruvate, *Sc*PDC$_{E477Q}$ was used (green triangles, PA, red squares, MAP, yellow inverse triangles, pyruvate, lines, sigmoid fit).

Figure 3

The overall structure of PDC tetramers representing MAP-*Kl*PDC and PYR-*Sc*PDC variants in **A**, and native *Kl*PDC[31] and PA-*Sc*PDC[32] in **B**.

The traces of Cα-atoms are shown with different colours for the individual subunits, loops 104-113 and 288-304 are presented as sticks (Figure A only), and the cofactor ThDP in space filling mode.

Figure 4

View of the regulatory sites with the activators bound covalently to residue C221 for MAP-*Kl*PDC (**A**) and PYR-*Sc*PDC$_{E477Q}$ (**B**).

The electron density is shown at a σ-level of 2.0 in the 2Fo-Fc map, amino acid residues in stick mode. The labelled residues can directly interact with the thiohemiketal. Labels in A correspond also to B.

Figure 5

Location of the histidine residues 114 and 115 at the active site of native *Kl*PDC (**A**) and pyruvate activated *Sc*PDC$_{D28A}$ (**B**).

Electron density is shown at a σ-level of 2.3 in the 2Fo-Fc map for ThDP and at a σ-level of 1.1 for the others (green, loop 104-113-H114-H115, wood, loop 288-304, yellow, C-terminal residues). All residues are presented in stick mode. The colours represent their B-factors (from low values, blue, to high values, red). Residues labelled with an asterisk belong to the other subunit within the same dimer.

Figure 6

Snapshots of the signal transduction pathway within one subunit.

For details, see section signal transfer. The outer edge of the subunit is visualised by a grey line. Only the residues mentioned in the text are shown, loop residues as sticks, all others in space filling mode. The asterisk labels residues of the other subunit of the same dimer. The secondary structure of the loops (red, α-helix, green, β-turn, white β-sheet) is illustrated. too.
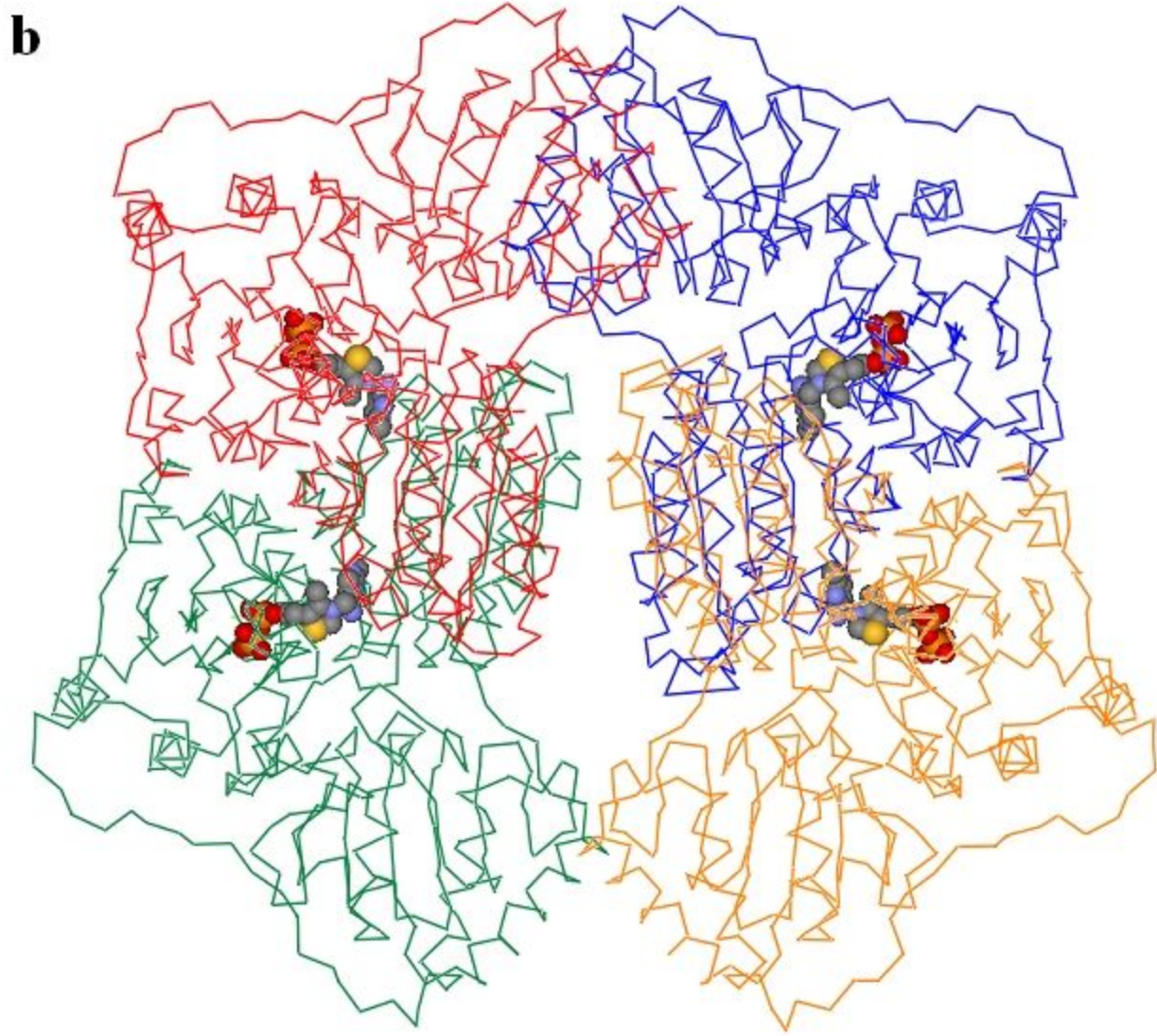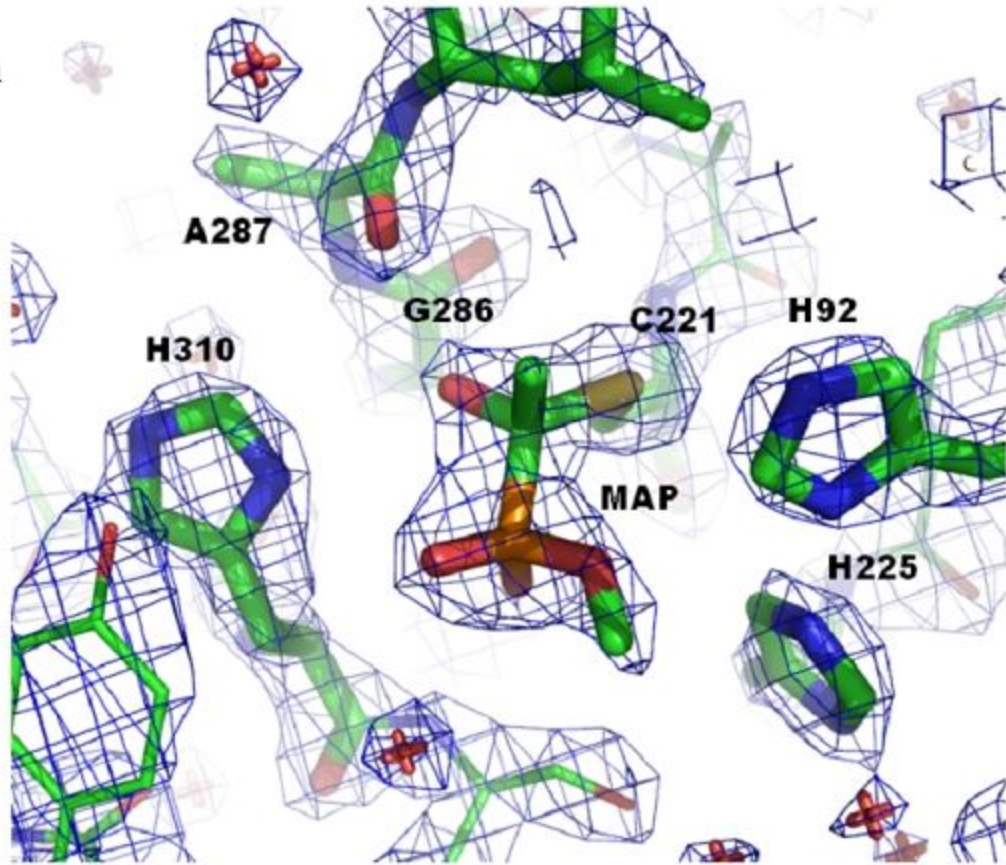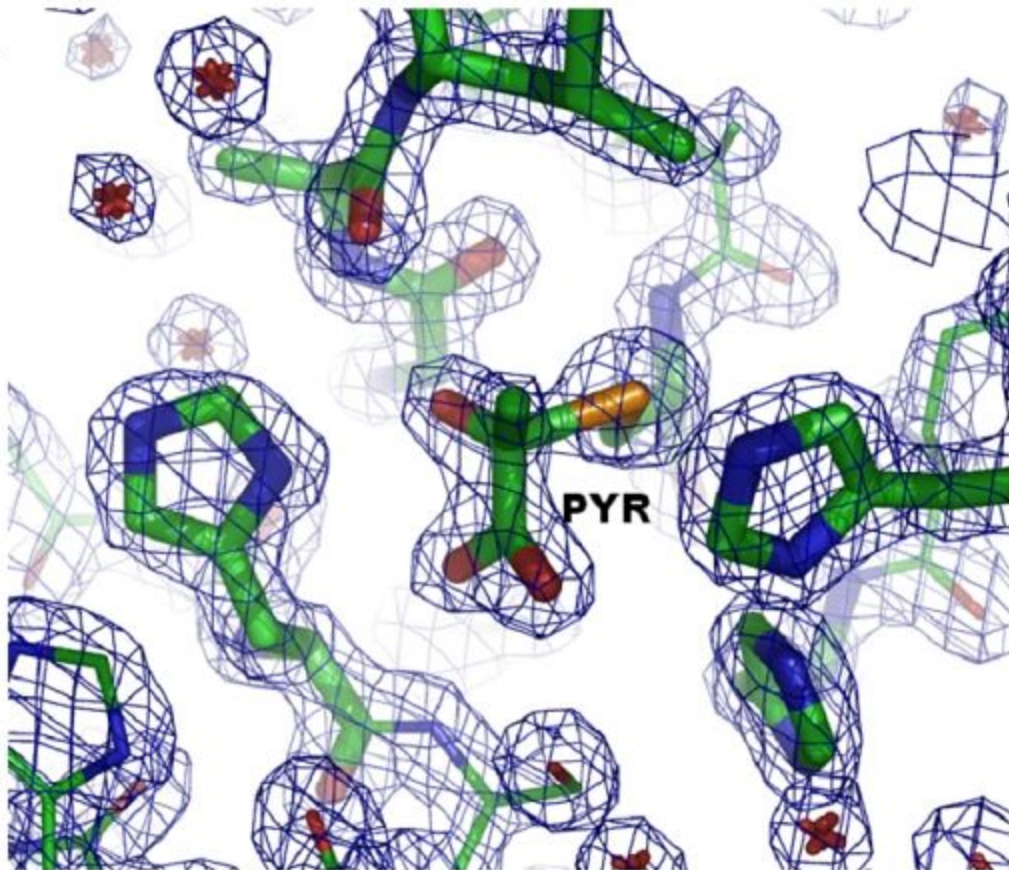
a

b

a

b

a

A287

G286   C221   H92

H310

MAP

H225

b

PYR

a

b

PYR

c

A287

d

f

H114*
PYR

H115*